CrossMark

Catalytic effect of lead oxide nano- and microparticles on thermal decomposition kinetics of energetic compositions containing TEGDN/NC/DAG

Vahid Mirzajani[1] · Khalil Farhadi[1] · Seied Mahdi Pourmortazavi[2]

Abstract The catalytic effect of lead oxide nano- and microparticles (PbO) on the thermal behavior and decomposition kinetics of energetic formulations composed of nitrocellulose (NC), triethyleneglycol dinitrate (TEGDN) and diaminoglyoxime (DAG) was investigated by simultaneous thermogravimetric analysis and differential scanning calorimetry. The results show that lead oxide nano- and microparticles could significantly alter thermal pattern of the studied energetic compositions. The effect of lead oxide content on thermal behavior of energetic compositions was also studied, and the results revealed that addition of different amounts of lead oxide caused to shift in the DSC peaks. Moreover, the catalyst decreases activation energy of the decomposition stage of energetic composition at about 20–40 kJ mol^{-1}. However, the catalyst enhances decomposition temperature of TEGDN/NC/DAG energetic compositions. By the aid of DSC data resulted by non-isothermal methods, the thermokinetic parameters such as activation energy (E_a), frequency factor (A), the critical ignition temperature of thermal explosion, the self-accelerating decomposition temperature (T_{SADT}) and also thermodynamic parameters of the studied energetic compositions were calculated and compared.

Keywords Lead oxide · Nanoparticles · Combustion catalyst · Kinetic parameters · TEGDN · Nitrocellulose · Energetic compositions · Thermal decomposition

✉ Seied Mahdi Pourmortazavi
pourmortazavi@yahoo.com

[1] Department of Analytical Chemistry, Faculty of Science, Urmia University, Urmia, Iran

[2] Faculty of Material and Manufacturing Technologies, Malek Ashtar University of Technology, Tehran, Iran

Introduction

Triethylene glycol dinitrate (TEGDN), which commonly utilized as an energetic plasticizer in propellant and explosive formulations, is a nitrated alcohol ester attained from the triethylene glycol. This energetic compound with the chemical structure shown in Scheme 1 is prepared as a pale yellow oily liquid [1]. Triethylene glycol dinitrate is somewhat similar to the nitroglycerin and commonly is being considered as a replacement for the nitroglycerin in the propellants due to its lower sensitivity. TEGDN/NC as an energetic mixture is composed of triethyleneglycol dinitrate and nitrocellulose, while this composition might be utilized in the double-base propellant formulations. Diaminoglyoxime (DAG), as an explosophore, is utilized in the rocket propellant compositions as an additive for providing both effects of ballistic modification and cooling [2–5]. Meanwhile, catalyst addition to the propellant formulations may improve their combustion performance effectively [6]. Lead compounds are widely utilized to achieve this aim and applied as the ballistic modifiers in the solid propellant compositions [7].

Transition metal oxides (TMOs) are imperative class of chemicals with the wide range of applications in various areas of material science, chemistry and physics [8]. TMOs such as PbO, CuO, Fe$_2$O$_3$ and TiO$_2$ are utilized in the production of propellants as catalyst. The particle size of TMOs is highly effective in their catalytic efficiency, while nano-sized TMOs could provide interested catalytic effects in the decomposition of energetic compositions [9–11]. Nano-sized TMOs unveil exclusive physicochemical properties than those of bulk and these nanoparticles have received considerable attention recently due to their catalytic, magnetic and electronic properties [8].

Scheme 1 Chemical structure
of triethylene glycol dinitrate
(TEGDN)
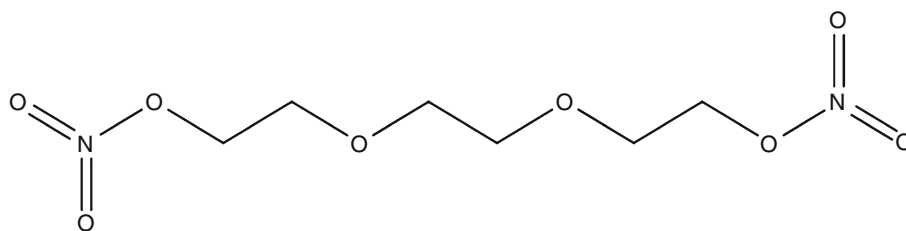
Nanomaterials have attained incredible attention due to their specific characteristics, i.e., high surface area, small pore size, and their possible production in three dimensional forms, which make enable their development as the advanced materials with the sophisticated applications [12]. Thus, investigation on the effect of nanoparticles on thermal behavior and decomposition kinetic of energetic formulations and compositions is vital in order to acquire valuable information about safe storage, handling and utilization of the compositions contained nanoparticles. This valuable knowledge could be resulted by thermal analysis systems, i.e., TG, DSC and DTA [13–26].

In this paper, effect of lead oxide nano- and microparticles as the combustion catalyst on decomposition reaction kinetic of the energetic formulation composed of triethyleneglycol dinitrate (TEGDN), nitrocellulose (NC) and diaminoglyoxime (DAG) was studied by TG–DSC systems under non-isothermal conditions. Also, an attempt was made in this study to determine thermokinetic parameters correspond to the thermal decomposition of the examined energetic compositions. This is hoped that the present study be helpful for future investigations on the characterization of the propellants composing TEGDN/NC/DAG.

Experimental

Materials

The fibrous NC polymer used in the present research was of commercial grade with about 12.0% nitrogen content [27]. TEGDN was prepared in the organic chemistry laboratory (MUT, Tehran) as proposed by refs. [28, 29]. Also, synthesis and purification of DAG [30] preparation of lead oxide nanoparticles [31, 32] were carried out, respectively, in the organic chemistry laboratory and inorganic chemistry laboratory (MUT, Tehran) as proposed previously. Lead oxide microparticles were purchased from Merck (Germany). The studied energetic sample (control sample or ES-1) was containing of 66% (by mass fraction) NC, 25% TEGDN, 3% centralite II and 6% DAG. Other energetic samples (ES-2, ES-3) and (ES-4, ES-5) were composed of similar components with previous sample, while either 1 or 3% PbO nano- or microparticles was introduced

to them and their NC content was reduced to 65 or 63%, respectively. The energetic samples were prepared homogeneously as proposed previously by Refs. [5, 7].

### FT-IR, NMR, SEM and XRD characterizations

Diaminoglyoxime was characterized after synthesis and purification by NMR and FT-IR techniques. NMR spectrum of the compound in DMSO was recorded on a BRUKER 250 MHZ spectrometer. The IR spectrum of DAG was obtained on a FT-IR spectrometer (PerkinElmer Spectrum model 1605) utilizing the KBr coins. Scanning electron microscope (Hitachi S4160) was applied to examine the morphology and particle size of synthesized lead oxide nanoparticles and the prepared energetic compositions. The X-ray powder diffraction (XRD) analysis was carried out on a Rigaku D/max 2500 V diffractometer equipped with a Cu target and a graphite monochromator.

TG–DSC studies

Thermal analyses of the energetic compositions were performed by a Mettler TA4000 thermal analyzer and a DSC (made by Mettler Toledo Co., Switzerland). The applied operation conditions during TGA analyses were as: the sample mass of about 4 mg; an alumina crucible; purging of N_2 gas with the flowing rate of 80 mL min^{-1}; heating rate (φ) of 10 °C min^{-1} at a temperature range of 50–400 °C. Meanwhile, the applied operating conditions for the DSC analyses were including: the sample mass of about 1.5 mg; an alumina crucible; 50 mL min^{-1} as flowing rate of N_2 purging in a temperature range of 50–300 °C.

Results and discussion

Chemical composition and structure of the synthesized and purified DAG were investigated by FT-IR and NMR techniques. FT-IR spectrum of DAG is observed in Fig. 1, while the typical functional groups of the compound are obvious the spectrum. The N–H_2 groups are responsible for the peaks at 3369.0, 3463.8 and 1665.3 cm^{-1}, while OH group are answerable for the observed peaks at 2800–3300
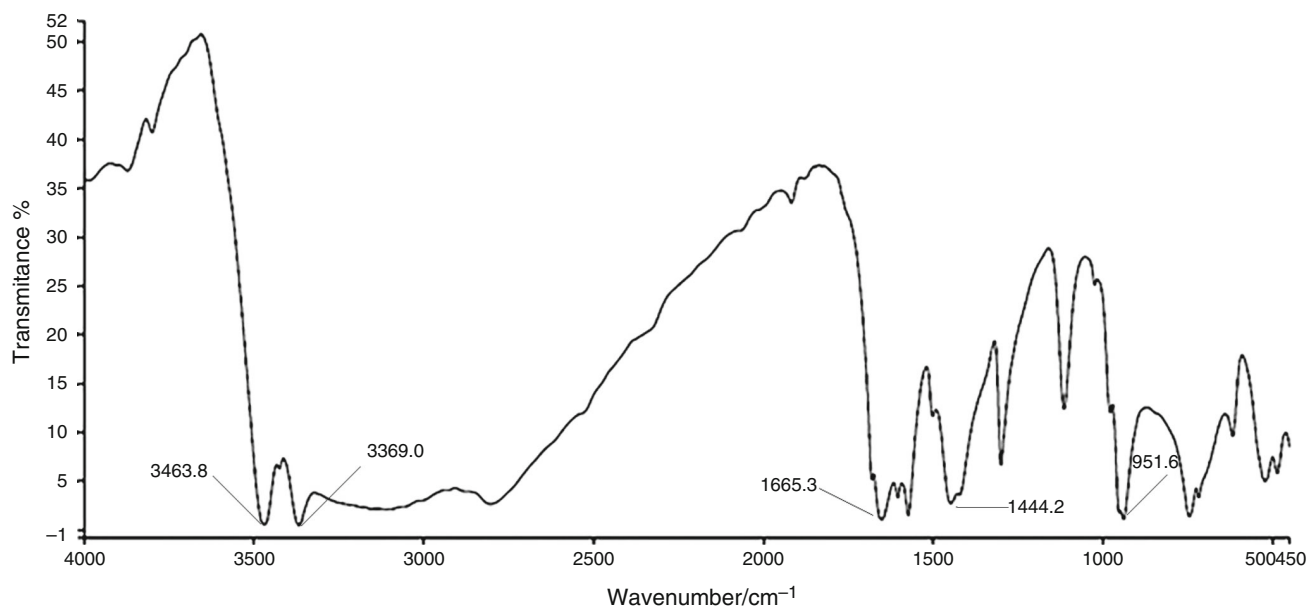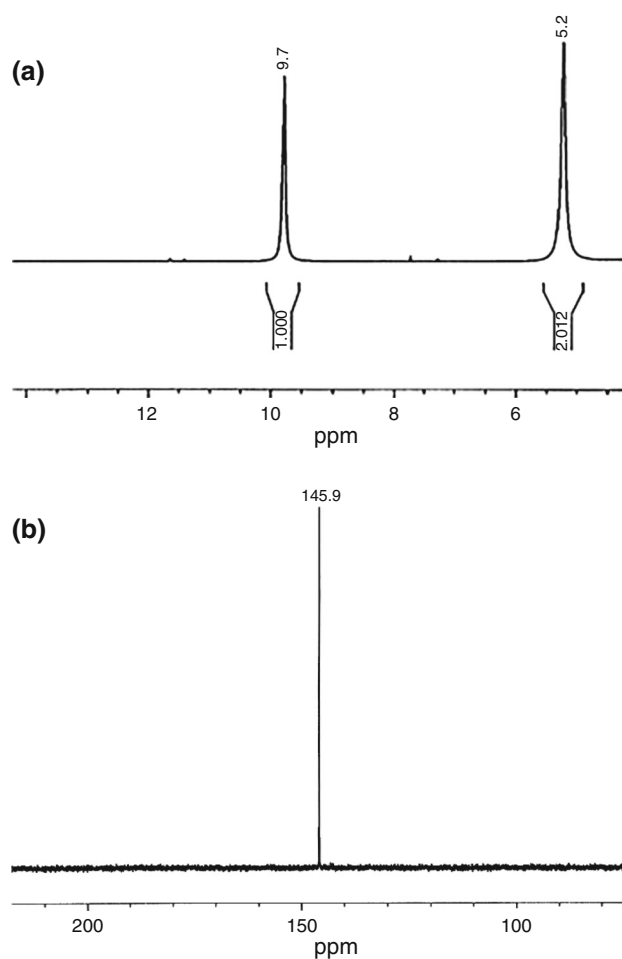
Fig. 1 FT-IR spectrum of the prepared DAG

and 1444.2 cm^{-1}. Furthermore, C = N and N–O groups are accountable for the appeared strong peaks at 1573.2 and 951.6 cm^{-1}, respectively.

^{1}H NMR spectrum of the DAG presented in Fig. 2a reveals two peaks at $\delta = 5.2$ ppm and $\delta = 9.7$ ppm attributed to the 4H in NH$_2$ and 2H in OH, respectively. On the other hand, ^{13}C NMR spectrum of the synthesized DAG presented in Fig. 2b exhibited a peak at 145.9 ppm which may be attribute to the bonding of NOH and NH$_2$ groups to the carbon atom.

Characterization of the prepared PbO nanoparticles

SEM image of the synthesized lead oxide nanoparticles is given in Fig. 3. As seen, the PbO nanoparticles possess a spherical geometry with an average diameter about 38 nm. Also, the XRD pattern of the prepared lead oxide nanoparticles is given in Fig. 4. As seen in this figure, all the diffraction peaks appeared in the resulted pattern are in agreement with the crystalline structure of the lead oxide from the diffraction software (JCPDS No 038-1477). The average crystallite size of product particles was calculated by Debye–Scherrer equation where in this equation (Eq. 1) D is accountable for the mean crystalline size, the X-ray wavelength (λ) for Cu Kα is equal to 1.5418 Å, β is corresponding to the full peak width at the half maximum (FWHM) and θ is attributed to the diffraction angle [33]. The results of calculation showed that the obtained PbO nanoparticles have an average crystalline size less than 40 nm.
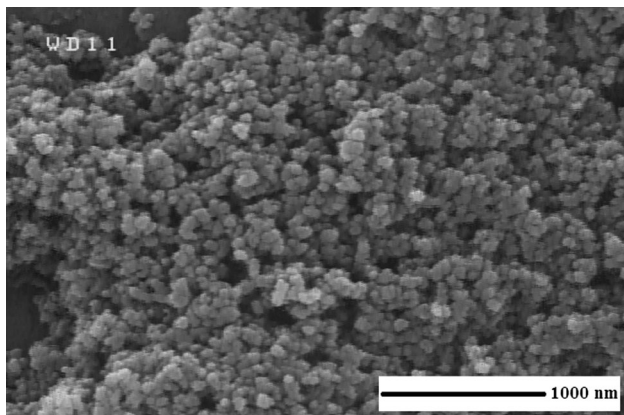

Fig. 2 a H-NMR spectrum of the prepared DAG. **b** C-NMR spectrum of the prepared DAG

$$D = \frac{0.9\lambda}{\beta \, \cos\theta} \tag{1}$$
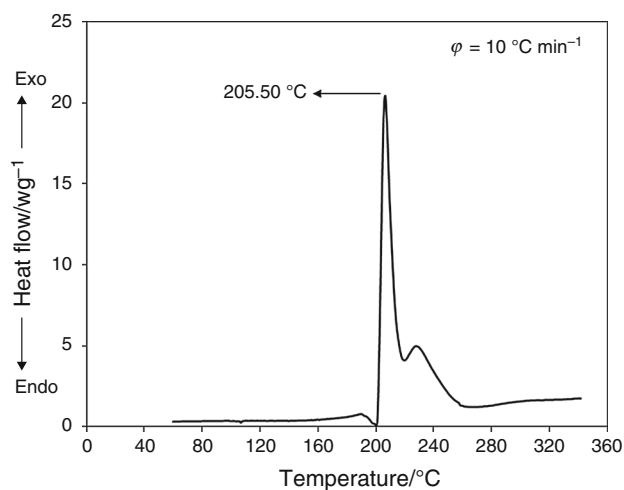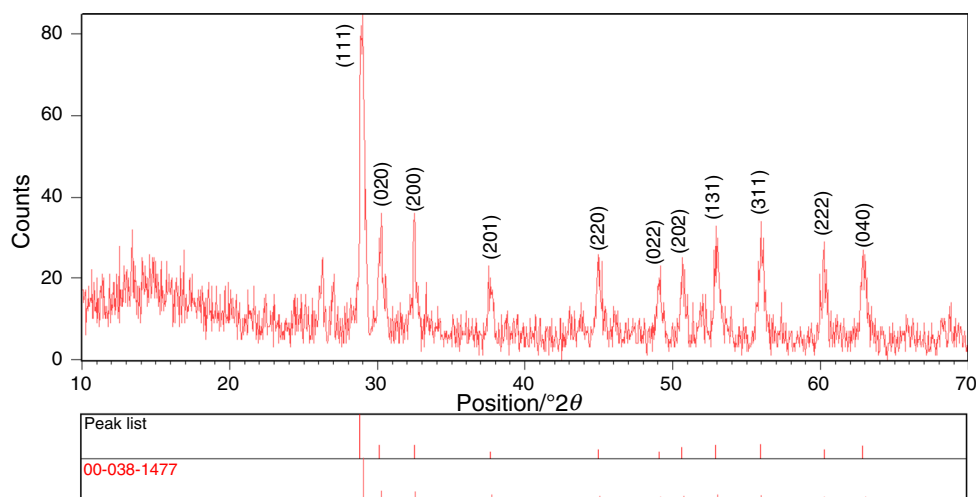
Thermal behavior of the pure components

Thermoanalytical curve of DAG presented in Fig. 5 shows an endothermic peak at about 200 °C corresponding to the melting phenomenon. However, DAG is decomposed exothermally at 205.5 °C, exactly after it's melting (at 200 °C). These results are compatible with previous report on DAG [34] which explained the occurrence of a main thermal degradation of DAG at the temperature ranges of 180–230 °C, simultaneous with the melting of the compound.

Thermal analysis result of the nitrocellulose sample (with 12.0% nitrate content) is given in Fig. 6. As seen, the DSC curve exhibits a single sharp exothermic behavior
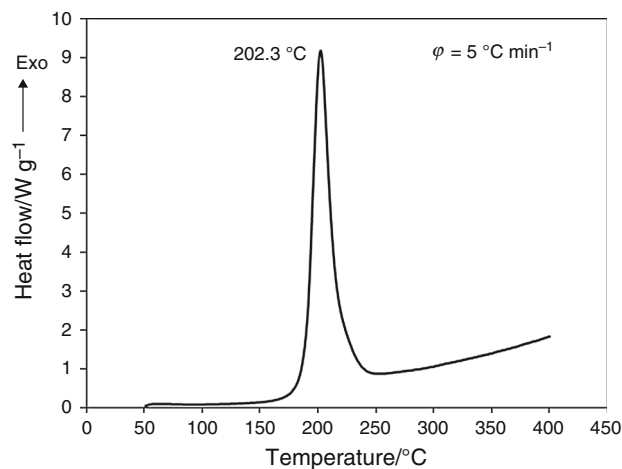

Fig. 5 DSC curve of the pure DAG

Fig. 3 SEM images of the prepared PbO nanoparticles

Fig. 6 DSC curve of the pure NC (with 12.0% nitrate content)

Fig. 4 XRD pattern of the prepared lead oxide nanoparticles
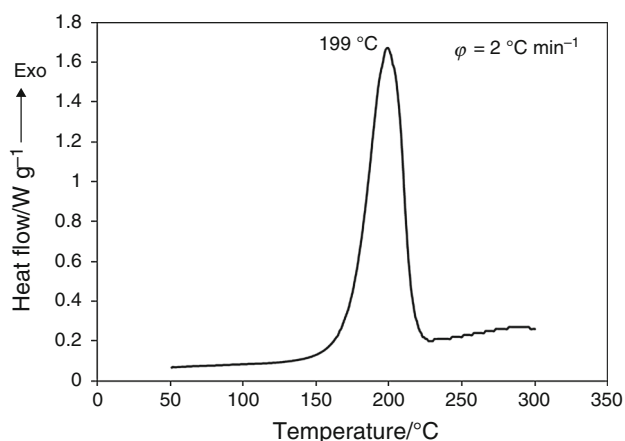
Fig. 7 DSC curve of the pure TEGDN

with a maximum temperature of 202.3 °C, which is in agreement with the previous study [27]. Meanwhile, the DSC curve of TEGDN, presented in Fig. 7, shows a single sharp exothermic peak during its decomposition with a maximum temperature of about 199 °C.

Characterization of the energetic compositions by SEM

Figure 8 shows the SEM images for the prepared energetic samples. SEM image of the energetic sample in the absence of PbO nanoparticles (Fig. 8a) shows that the sample is homogeneous and no agglomeration of the ingredients was observed. On the other hand, Fig. 8b, c present the SEM images for the energetic samples containing 1 and 3% PbO nanoparticles (ES-2 and ES-3), respectively. As seen in the SEM images, the nanoparticles are distributed through the samples uniformly and no considerable agglomeration of the ingredients was observed.

Catalytic effect of PbO nano- and microparticles on thermal behavior of energetic compositions

The results of this report reveal the catalytic effect of lead oxide particles as additive on the thermal behaviors of TEGDN/NC/DAG energetic compositions. It has been reported [35, 36] that metal compounds could yield two types of catalytic effects: (a) positive catalytic effect, which increases the burning rate and in contrast lowers the required activation energy for initiating thermal decomposition of the composition, and (b) negative catalysts, which exhibit a reverse trend. Previous researches performed about catalytic effect of metal compounds shows diverse influences on burning rate and thermal decomposition of the energetic compositions [36, 37]. In this work, the catalytic activity of the nano- and microparticles on
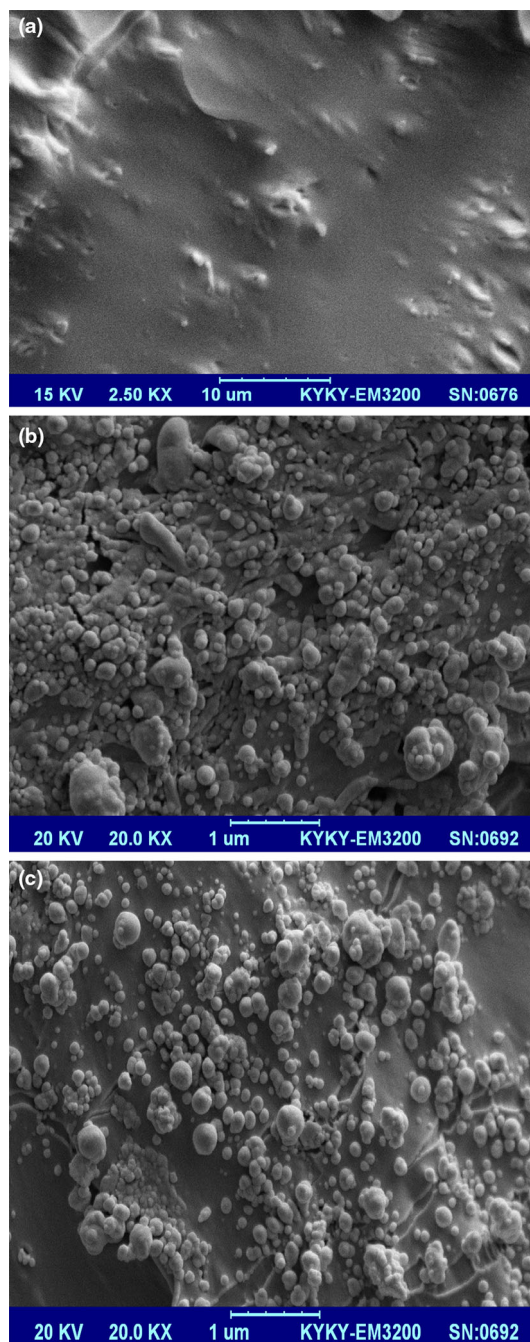
Fig. 8 SEM images of the investigated energetic samples **a** without PbO nano- and microparticles, **b** with 1% PbO nanoparticles and **c** with 3% PbO nanoparticles

thermal decomposition of TEGDN/NC/DAG energetic composition was studied by thermal analysis. TG–DSC curves of the investigated energetic compositions at the heating rate of 10 °C min^{-1} are shown in Fig. 9. In Fig. 9a thermal pattern of TEGDN/NC/DAG sample in the absence of lead oxide (ES-1) is given, which exhibits a single mass loss stage starting from 194.7 °C. The maximum DSC peak temperature of 196.6 °C with the mass loss about 80.3% is

observed for this stage. DSC curve of the energetic sample containing 1% PbO nanoparticles (ES-2) shows a sharp exothermic event with the onset temperature of 196.6 °C and maximum peak temperature of 199.8 °C; while TG analysis of the sample reveals a mass loss of about 77.0%

for this stage (Fig. 9b). DSC curve of the sample containing 3% PbO nanoparticles (ES-3) shows similarly a sharp exothermic behavior which starts from 195.4 °C and maximizes at the temperature of 200.5 °C; also the mass loss of the sample at this stage is about 73.5%. (Figure 9c).
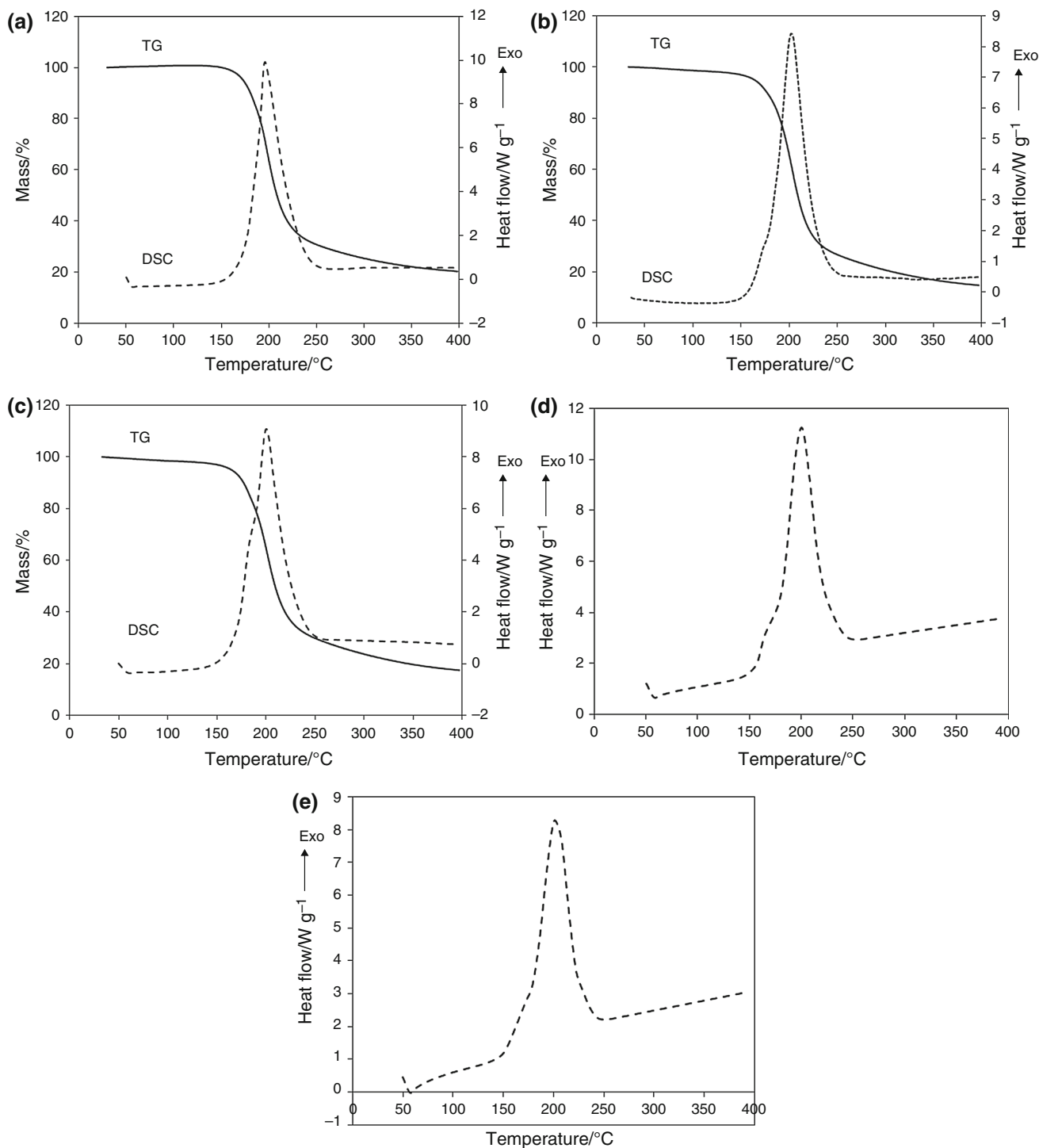
Fig. 9 TG/DSC curves for energetic samples at heating rate of $10°\text{C min}^{-1}$ in N_2 atmosphere: **a** control sample or ES-1, **b** control sample + 1% nano-PbO or ES-2, **c** control sample + 3% nano-PbO or ES-3, **d** control sample + 1% micro-PbO or ES-4, **e** control sample + 3% micro-PbO or ES-5

DSC curve of the sample containing 1% PbO microparticles (ES-4) shows similarly a sharp exothermic behavior which starts from 177.8 °C and maximizes at the temperature of 199.1 °C. (Figure 9d); also DSC curve of the sample containing 3% PbO microparticles (ES-5) shows similarly a sharp exothermic behavior which starts from 176.5 °C and maximizes at the temperature of 201.6 °C. (Figure 9e). A summary of DSC results for TEGDN/NC/DAG energetic compositions containing different amounts of PbO nano- and microparticles are also presented in Table 1. According to the DSC data, it could be concluded that both nano- and micro-PbO particles enhance the decomposition temperature of TEGDN/NC/DAG energetic composition. By comparing the maximum peak temperature of the investigated energetic samples in presence of nano- and micro-PbO; generally it is obvious that there is no significant difference between thermal decomposition temperatures of TEGDN/NC/DAG energetic composition modified with nano- and microparticles.

Addition of PbO catalyst (either micro or nano) to the samples efficiently decreases the heat of decomposition for the energetic composition. Nevertheless, increasing of PbO catalyst contents (either micro or nano) in the samples slightly decreases the heat of decomposition released from this energetic composition. The described trend in the decrement of the heat of decomposition is shown in Fig. 10. As seen in this figure, the energetic sample in the absence of PbO catalyst has the highest heat of decomposition while the sample containing 3% of the nano-catalyst has the lowest.

Effect of DSC heating rate on decomposition of energetic samples

Figure 11 presents DSC curves for decomposition of the studied energetic samples at different heating rates (i.e., 2, 5, 7 and 10 °C min⁻¹). As seen in this figure, decomposition peaks of the samples were shifted to the higher temperatures by increasing the heating rate. Table 1 shows these shifts in the peak temperatures quantitatively.

Table 1 Maximum peak temperature of the investigated energetic samples at different heating rates

Heating rate/°C min⁻¹	Decomposition temperature/°C				
	ES-1	ES-2	ES-3	ES-4	ES-5
2	182.9	181.9	184.8	181.2	184.9
5	187.2	191.3	189.7	188.7	194.0
7	192.5	195.9	193.1	193.7	198.6
10	196.6	199.8	200.5	199.1	201.6
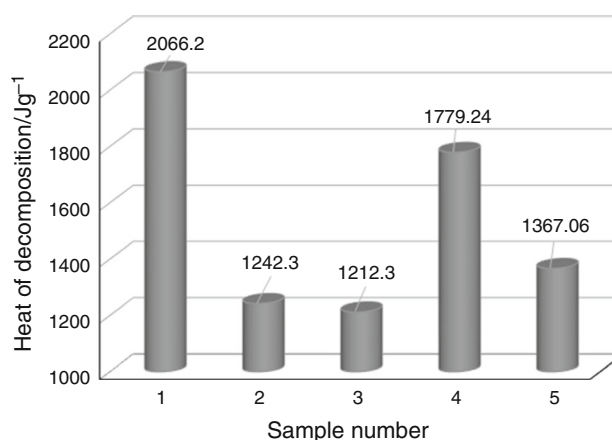
Fig. 10 The heats of decomposition for the energetic samples (the values are resulted from the average DSC exothermic peak areas obtained at various heating rates)

Kinetic parameters for thermal decomposition of energetic samples

The involved processes during solid-state decomposition reactions generally are complex and their thermokinetic parameters could be determined by some well-known methods, i.e., Kissinger, Starink and Ozawa–Flynn–Wall (O.F.W.) [38–48]. These methods were jointly employed in the present study to calculate the Arrhenius parameters, i.e., activation energy (E_a) and pre-exponential factor (A) based on the DSC data for the studied energetic samples. The first utilized method for determining the Arrhenius parameters was Kissinger [38–43], in which the activation energy is obtained as follow (Eq. 2):

$$\text{Ln} \frac{\varphi}{T_m^2} = \text{Ln} \frac{AR}{E_a} - \frac{E_a}{R\,T_m} \tag{2}$$

While, φ is the DSC heating rate, T_m is the temperature of the DSC peak at maximum heat flow, and R is the universal gas constant. The activation energies for the studied energetic samples were obtained by DSC data resulted at different heating rates (Table 1). The results of drawing $\text{Ln}\left(\frac{\varphi}{T_m^2}\right)$ against $1/T_m$ were linear plots for all studied samples, which confirm thermal decomposition of the samples undergoes no distinction at different applied heating rates [44–46]. Meanwhile, the slope of these linear plots was equal to $-E_a/R$. In the next step, the Arrhenius factor or log (A/S^{-1}) was calculated via following equation recommended by ASTM E698 (Eq. 3) [47] using the calculated value of activation energy (E_a).

$$A = \frac{[\varphi E_a \exp\left(\frac{E_a}{RT_m}\right)]}{R T_m^2} \tag{3}$$
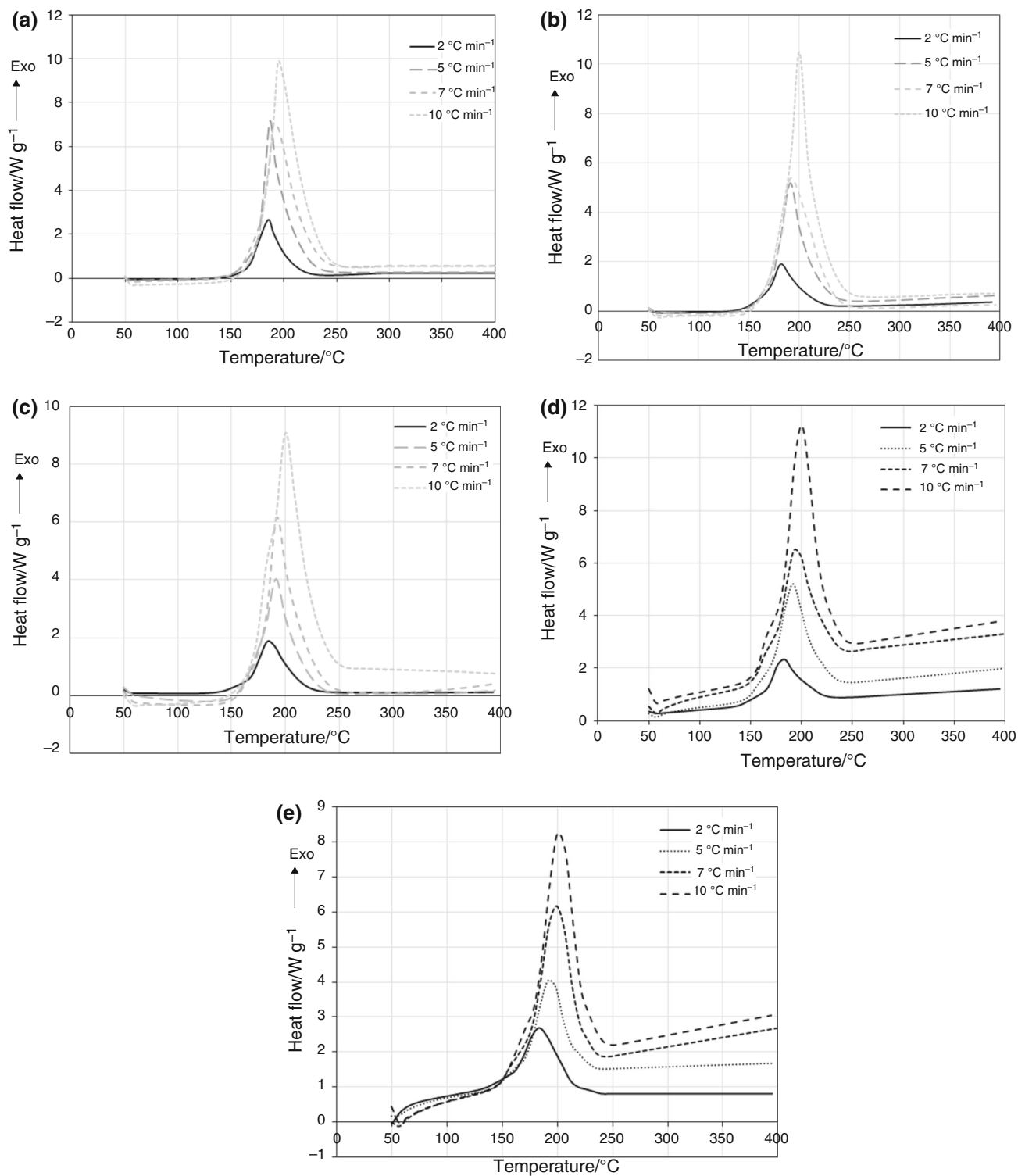
Fig. 11 Effect of DSC heating rate on decomposition temperature of investigated energetic samples: **a** control sample (ES-1); **b** control sample in the presence of 1% nano-PbO (ES-2); **c** control sample in the presence of 3% nano-PbO (ES-3); **d** control sample in the presence of 1% micro-PbO (ES-4); **e** control sample in the presence of 3% micro-PbO (ES-5)

The resulted values of the activation energy and Arrhenius factor for the studied energetic samples are presented in Table 2. On the other hand, activation energy

(E_a) values for these energetic samples were computed via Starink method [48] by the aid of Eq. 4. In this method, the plot of $Ln\left(\varphi \ T_m^{-1.92}\right)$ against the inverse of maximum peak

Table 2 Comparison of kinetic parameters for thermal decomposition of energetic samples obtained by Kissinger, Starink and O.F.W. methods

Sample	Method	E_a/kJ mol^{-1}	Log/A/s^{-1}	r	Q
ES-1	Kissinger	190.4	19.4	0.9620	0.2223
	Starink	190.6	19.4	0.9621	0.2223
	O.F.W.	188.3	19.2	0.9648	0.2222
ES-2	Kissinger	151.7	14.9	0.9989	0.0364
	Starink	151.9	14.9	0.9989	0.0364
	O.F.W.	151.6	14.8	0.9991	0.0362
ES-3	Kissinger	171.0	17.1	0.9441	0.2787
	Starink	171.1	17.1	0.9477	0.2806
	O.F.W.	169.9	16.9	0.9434	0.2804
ES-4	Kissinger	152.0	14.9	0.9860	0.1286
	Starink	152.2	15.0	0.9861	0.1288
	O.F.W.	151.8	14.9	0.9873	0.1339
ES-5	Kissinger	162.7	16.0	0.9980	0.0501
	Starink	162.9	16.0	0.9980	0.0501
	O.F.W.	162.1	15.9	0.9981	0.0511

r Linear regression

Q Standard mean square deviation

temperature at different heating rates permits the prediction of the activation energy. Fortunately, this method is usable for computing the activation energy by the aid of following equation, neglected of a accurate knowledge about the reaction mechanism:

$$\mathrm{Ln}\left(\frac{\varphi}{T_m^{1.92}}\right) + 1.0008\,\frac{E_a}{RT_m} = C \tag{4}$$

The results of drawing of Ln ($\varphi\,T_m^{-1.92}$) against reverse of peak temperature at maxima for the studied energetic samples were straight lines, while their slopes were utilized to calculate the values of the activation energy. Meantime, the corresponded values of Arrhenius factor (A) for each of these energetic samples were obtained by Eq. (3) [49]. Also, Ozawa–Flynn–Wall (O.F.W.) as the third method was employed to predict the values of activation energy (E_a) for the studied energetic samples. This method is based on the kinetics equations utilized for the heterogeneous chemical reactions and could be presented as Eq. 5 [49–51]. As seen in this equation, plotting of the heating rate logarithm against the converse of the maximum peak temperatures resulted by different DSC peaks at various heating rates permits the computation of the activation energy. In this method, similar to the previous methods, determination of the activation energy without an exact knowledge about the reaction mechanism is possible via utilizing Eq. 5.

$$\log\varphi = \log\frac{A\,E_a}{R\,g(\alpha)} - 2.315 - 0.4567\,\frac{E_a}{RT_m} \tag{5}$$

In this equation, $g(\alpha)$ represents integral function of the conversion. O.F.W. is a multiple scanning method and belongs to the model-free isoconventional approaches; thus, this method allows predicting of the activation energy independently [49]. Also, the values of Arrhenius factor (A) for the energetic samples were computed by Eq. (3) [52–54]. Table 2 gives the resulted values of activation energy (E_a) and Arrhenius factor (log A) for decomposition of the investigated energetic samples calculated by Kissinger, Starink and O.F.W. methods for comparison. In fact, the presented data in this table are helpful for checking the validity and constancy of the values of activation energy obtained by different methods. As seen in this table, the activation energies and Arrhenius factors computed by Kissinger method for decomposition of the energetic samples are comparable with those resulted by Starink and O.F.W. methods. However, the computed values by O.F.W. method are faintly lower than those resulted by two other methods. Totally, these results confirm the reliability of the calculations. The resulted kinetic data point out that TEGDN/NC/DAG energetic compositions treated with (micro or nano) PbO catalyst have lower activation energy values and thus require lower energy for initiating of their decomposition reaction. In fact, positive catalytic effect of PbO particles lowers the required energy for initiation of the reaction and later increases the burning rate [55]. Therefore, PbO catalyst is capable to reduce the energetic barrier for commencing of the reactions and hence leads to acceleration of the decomposition process [56]. Meantime, comparing catalytic effect of micro- and nanoparticles of lead oxide on the thermal decomposition of TEGDN/NC/DAG energetic composition shows that PbO microparticles have lower positive catalytic effect on the thermal decomposition of energetic compositions in comparison with PbO nanoparticles, while this behavior may arise from the specific characteristics of nanoparticles, i.e., small particle size and high surface area.

In addition, the thermodynamic parameter values corresponding to the thermal activation of the studied energetic samples are calculable utilizing the following equations [57–60]. Thus, Eqs. 6–8 were utilized to predict the values of activation entropy ($\Delta S^{\#}$), activation enthalpy ($\Delta H^{\#}$) and free energy of activation ($\Delta G^{\#}$).

$$A\exp\frac{-E_a}{RT} = v\exp\frac{-\Delta G^{\neq}}{RT} \tag{6}$$

$$\Delta H^{\neq} = E_a - RT \tag{7}$$

$$\Delta G^{\neq} = \Delta H^{\neq} - T\Delta S^{\neq} \tag{8}$$

In Eq. 6, $v = K_B T/h$ (while h and K_B symbolized Plank and Boltzmann constants, respectively). Table 3 presents the resulted values for the thermodynamic parameters corresponding to the studied energetic samples. As seen in this table, the positive values of $\Delta H^{\neq}$ and $\Delta G^{\neq}$ for the energetic samples confirm that their decomposition reactions are non-spontaneous and initiation of their reactions requires introducing of the heat.

Calculation of decomposition reaction rate constant

The rate constant for decomposition reaction (k) of the energetic samples was computed by Eq. (9). The order of decomposition reaction for the studied energetic samples was assumed as the first order [61]:

$$\log k = \log A - \frac{E_a}{2.3RT} \tag{9}$$

The values of reaction rate constant (k) for the energetic samples were computed by the use of activation energy (E_a) and Arrhenius factor (A) values resulted by different methods (i.e., Kissinger, Starink and O.F.W.) at 25 °C as the environment temperature. Table 3 gives the resulted values of $\log k$ for the energetic samples. By comparing of the reaction rate constant values, it could be found that the modified energetic samples with PbO nano- and microparticles (ES-2 to ES-5) have reaction rate constants considerably higher than that the energetic sample without lead oxide treatment (control sample or ES-1). These values of $\log k$ for the energetic samples confirm that both PbO nano- and microparticles have catalytic effects on the decomposition of the energetic samples and increase their decomposition reaction rate.

Critical ignition temperature

The safe storage and process of the studied energetic compositions require knowledge about another significant

factor which is known as the critical ignition temperature (T_b). This factor shows the maximum temperature at which the composition undergoes a thermal runaway [46, 52]. This temperature for each composition is predictable based on the burning theory, while some thermokinetic parameters, i.e., activation energy, Arrhenius factor and heat of reaction are essential. In the present study, the critical temperatures corresponding to the thermal explosion (T_b) of the energetic samples were obtained via Eqs. (10–11) as follows [62, 63]:

$$T_e = T_{e0} + b\varphi_i + c\varphi_i^2, \quad i = 1 - 4 \tag{10}$$

$$T_b = \frac{E_a - \sqrt{E_a^2 - 4E_a R T_{p0}}}{2R} \tag{11}$$

In Eq. 10, b and c are the coefficients, while R is the universal gas constant. T_{e0} is commonly called self-accelerating decomposition temperature (T_{SADT}), while this symbol is attributed to the onset temperature (T_e) while $\varphi \rightarrow 0$ and computed by Eq. (10). However, the resulted values were utilized for computation of critical temperatures. The resulted temperatures are given in Table 3.

Comparison thermal stability of investigated energetic samples

TG/DSC curves for the investigated energetic samples in the absence and/or presence of the nano- and micro-PbO are presented in Fig. 9. The blank sample (ES-1 which has no PbO content) and the modified samples with nano- and micro-PbO (ES-2 and ES-3 containing 1 and 3% nanoparticles and ES-4 and ES-5 containing 1 and 3% microparticles, respectively) present similar thermal patterns, and all of them display a single exothermic event during their thermal decomposition. However, the resulted curves showed that thermal decomposition of the energetic samples modified with nano- and micro-PbO occurred at the higher temperatures. On the other hand, by comparison thermal stability of the blank sample (ES-1) with the samples containing nano- and micro-PbO, it was appeared that the modified samples with nano- and microparticles have lower activation energy about 20–40 kJ mol⁻¹. It means that introducing of nano- and micro-PbO makes the decomposition of TEGDN/NC/DAG energetic composition more easily. However, comparing of the maximum peak temperature of the investigated energetic samples in the presence of nano- and micro-PbO shows that there is not significant difference between thermal decomposition temperatures, activation energies and frequency factors of TEGDN/NC/DAG energetic composition modified with nano- and microparticles.

Table 3 Thermodynamic data for decomposition of the studied energetic samples

Sample	$\Delta G^{\neq}/$ kJ mol⁻¹	$\Delta H^{\neq}/$ kJ mol⁻¹	$\Delta S^{\neq}/$ J mol⁻¹	Log k	$T_b/$ °C	$T_{SADT}/$ °C
ES-1	129.6	186.6	123.9	−13.9	196.2	172.9
ES-2	131.5	148.0	36.9	−11.7	185.5	140.8
ES-3	131.3	167.2	79.2	−12.8	190.9	144.3
ES-4	134.6	148.3	30.3	−11.6	189.1	208.0
ES-5	136.1	159.0	50.7	−12.4	189.4	175.9

Conclusions

The effect of PbO nano- and microparticles on thermal decomposition of TEGDN/NC/DAG energetic compositions was investigated via simultaneous differential scanning calorimetery (DSC) and thermogravimetery (TG) techniques. Thermokinetic and thermodynamic parameters corresponding to the decomposition of different energetic compositions were computed based on their DSC curves. The values of the activation energy and frequency factor for the studied energetic compositions were computed by some well-known methods. The results of this study show that the decomposition temperature of the energetic compositions in the presence of nano- and micro-PbO is higher than the similar composition without PbO particles. However, the energetic samples containing nano- and micro-PbO possess lower frequency factors and activation energies. There is no significant difference between thermal decomposition temperatures and activation energy values of TEGDN/NC/DAG energetic composition modified with nano- and microparticles. Besides, lower values of the critical ignition temperature (T_b) and the self-accelerating decomposition temperature (T_{SADT}) of the energetic samples in the presence of nanoparticles show higher sensitivity of the energetic samples containing PbO nanoparticles in comparing samples modified with the microparticles. Based on the results of this study it could be concluded that the addition of PbO (either nano- or microparticles) has a considerable effects on thermal behavior of TEGDN/NC/DAG energetic compositions, while PbO particle size has no substantial diverse effects on thermal decomposition of these energetic samples.

References

1. Kanno H, Yamamoto H. (1995) US Patent 5476967.
2. Takahashi PM, Netto AVG, Mauro AE, Frem RCG. Thermal study of nickel(II) pyrazolyl complexes. J Therm Anal Calorim. 2005;79:335–8.
3. Stoner CE Jr, Brill TB. Thermal decomposition of energetic materials 46. The formation of melamine-like cyclic azines as a mechanism for ballistic modification of composite propellants by DCD, DAG, and DAF. J Combust Flame. 1991;83:302–8.
4. Talawar MB, Makashir PS, Nair JK, Pundalik SM, Mukundan T, Asthana SN, Singh SN. J Hazard Mater. 2005;A 125:17–22.
5. Williams GK, Palopoli SF, Brill TB. Thermal decomposition of energetic materials 65. Conversion of insensitive explosives (NTO, ANTA) and related compounds to polymeric melon-like cyclic azine burn-rate suppressants. J Combust Flame. 1994;98:197–204.
6. Ravanbod M, Pouretedal HR. Catalytic effect of Fe_2O_3, Mn_2O_3, and TiO_2 nanoparticles on thermal decomposition of potassium nitrate. J Therm Anal Calorim. 2016;124:1091–8.
7. Yi JH, Zhao FQ, Hong WL, Xu SY, Hu RZ, Chen ZQ, Zhang LY. Effects of Bi-NTO complex on thermal behaviors, nonisothermal reaction kinetics and burning rates of NG/TEGDN/NC propellant. J Hazard Mater. 2010;176:257–61.
8. Nayak H, Jena AK. Catalyst effect of transition metal nano oxides on the decomposition of lanthanum oxalate hydrate: a thermogravimetric study. Int J Sci Res (IJSR). 2014;3: 381–8.
9. Martins S, Fernandes JB, Mojumdar SC. Catalysed thermal decomposition of $KClO_3$ and carbon gasification. J Therm Anal Cal. 2015;119:831–5.
10. Kapoor IPS, Srivastava P, Singh G. Nanocrystalline transition metal oxides as catalysts in the thermal decomposition of ammonium perchlorate. Propellants Explos Pyrotech. 2009;34:351–6.
11. Mahinroosta M. Catalytic effect of commercial nano-CuO and nano-Fe_2O_3 on thermal decomposition of ammonium perchlorate. J Nanostruct Chem. 2013;3:1–6.
12. Shahidzadeh M, Shabihi P, Pourmortazavi SM. Sonochemical preparation of copper(II) chromite nanocatalysts and particle size optimization via Taguchi method. J Inorg Organomet Polym. 2015;25:986–94.
13. Shamsipur M, Pourmortazavi SM, Roushani M, Miran Beigi AA. Thermal behavior and non-isothermal kinetic studies on titanium hydride-fueled binary pyrotechnic compositions. Combust Sci Technol. 2013;185:122–33.
14. Rogers RN, Smith LC. Estimation of preexponential factor from thermal decomposition curve of a weighed sample. J Anal Chem. 1967;39:1024.
15. Mohan Murali BK, Ganesan V, Rao KB, Mohan VK. Hazard characteristics of isosorbide dinitrate-lactose mixtures. J Hazard Mater. 1979;3(2):177–82.
16. Sunitha M, Reghunadhan Nair CP, Krishnan K, Ninan KN. Kinetics of Alder-ene reaction of Tris (2-allylphenoxy) triphenoxycyclotriphosphazene and bismaleimides-a DSC study. Thermochim Acta. 2001;374:159–69.
17. Turcotte R, Vachon M, Kwok QSM, Wang R, Jones DEG. Thermal study of HNIW (CL-20). Thermochim Acta. 2005;433:105–15.
18. Pourmortazavi SM, Sadri M, Rahimi-Nasrabadi M, Shamsipur M, Jabbarzade Y, Shafaghi Khalaki M, Abdollahi M, Shariatinia Z, Kohsari I, Atifeh SM. Thermal decomposition kinetics of electrospun azidodeoxy cellulose nitrate and polyurethane nanofibers. J Therm Anal Cal. 2015;119:281–90.
19. Azimfar F, Kohsari I, Pourmortazavi SM. Investigation on decomposition kinetic and thermal stability of metallocene catalysts. J Inorg Organomet Polym. 2009;19:181–6.
20. Om Reddy G, Srinivasa Rao A. Stability studies on pentaerytritol tetranitrate. Propellants Explos Pyrotech. 1992;17:307.
21. Miran Beigi AA, Abdouss M, Yousefi M, Pourmortazavi SM, Vahid A. Investigation on physical and electrochemical properties of three imidazolium based ionic liquids (1-hexyl-3-methylimidazolium tetrafluoroborate, 1-ethyl-3-methylimidazolium bis(trifluoromethylsulfonyl) imide and 1-butyl-3-methylimidazolium methylsulfate). J Mol Liq. 2013;177: 361–8.
22. Mirzaei M, Lippolis V, Carla Aragoni M, Ghanbari M, Shamsipur M, Meyer F, Demeshko S, Pourmortazavi SM. Extended structures in copper(II) complexes with 4-hydroxypyridine-2,6-dicarboxylate and pyrimidine derivative ligands: x-ray crystal structure, solution and magnetic studies. Inorg Chim Acta. 2014;418:126–35.
23. Shamsipur M, Miran Beigi AA, Teymouri M, Pourmortazavi SM, Irandoust M. Physical and electrochemical properties of ionic liquids 1-ethyl-3-methylimidazolium tetrafluoroborate, 1-butyl-3-methylimidazolium trifluoromethanesulfonate and 1-butyl-1-methylpyrrolidinium bis(trifluoromethyl-sulfonyl) imide. J Mol Liq. 2010;157:43–50.

24. Singh G, Kapoor IPS, Mannan SM, Kaur J. Studies on energetic compounds, Part 8: thermolysis of salts of HNO_3 and $HClO_4$. J Hazard Mater. 2000;A79:1–18.

25. Zeman S. New aspects of initiation reactivities of energetic materials demonstrated on nitramines. J Hazard Mater. 2006;A132:155–64.

26. Keshavarz MH. Simple method for prediction of activation energies of the thermal decomposition of nitramines. J Hazard Mater. 2009;162:1557–62.

27. Pourmortazavi SM, Rahimi-Nasrabadi M, Rai H, Besharati-Seidani A, Javidan A. Role of metal oxide nanomaterials on thermal stability of 1,3,6-trinitrocarbazole. Propellants Explos Pyrotech. 2016;41:912–8.

28. Nicholas A, Alexander J, Michael P. (2012) US Patent 20120130115A1.

29. Gouranlou F, Kohsari I. Synthesis and characterization of 1,2,4-butanetrioltrinitrate. J Asian J Chem. 2010;22:4221–8.

30. Park DJ, Stern AG, Willer RL. A convenient laboratory preparation of cyanogen. Synth Commun. 1990;20:2901–6.

31. Karami H, Karimi MA, Haghdar S, Sadeghi A, Mir-Ghasemi R, Mahdi-Khani S. Synthesis of lead oxide nanoparticles by Sonochemical method and its application as cathode and anode of lead-acid batteries. J Mater Chem Phys. 2008;108(2):337–44.

32. Karami H, Karimi MA, Haghdar S. Synthesis of uniform nanostructured lead oxide by sonochemical method and its application as cathode and anode of lead-acid batteries. Mater Res Bull. 2008;43(11):3054–65.

33. Fazli Y, Pourmortazavi SM, Kohsari I, Sadeghpur M. Electrochemical synthesis and structure characterization of nickel sulfide nanoparticles. J Mater Sci Semicond Process. 2014;27:362–7.

34. Pourmortazavi SM, Farhadi K, Mirzajani V, Mirzajani S, Kohsari I. Study on the catalytic effect of diaminoglyoxime on thermal behaviors, non-isothermal reaction kinetics and burning rate of homogeneous double-base propellant. J Therm Anal Calorim. 2016;125:121128.

35. Kubota N. Propellants and explosives, chapter 7. New York: Wiley; 2007. p. 195–8.

36. Preckel RF. Plateau ballistics in NC propellant. ARS J. 1961;31:1286–7.

37. Joshi AD, Singh H. Effect of certain lead and copper compounds as ballistic modifier for double base rocket propellants. J Energy Mater. 1992;10(4–5):299–309.

38. Kissinger HE. Reaction kinetics in differential thermal analysis. J Anal Chem. 1957;29:1702–6.

39. Pourmortazavi SM, Hosseini SG, Rahimi-Nasrabadi M, Hajimirsadeghi SS, Momenian H. Effect of nitrate content on thermal decomposition of nitrocellulose. J Hazard Mater. 2009;162:1141–4.

40. Ma H-X, Song J-R, Hu R-Z. Non-isothermal kinetics of the thermal decomposition of 3-nitro-1,2,4-triazol-5-one magnesium complex. Chin J Chem. 2003;21(12):1558–61.

41. Hu R-Z, Chen S-P, Gao S-L, Zhao F-Q, Luo Y, Gao H-X, Shi Q-Z, Zhao H-A, Yao P, Li J. Thermal decomposition kinetics of $Pb_{0.25}Ba_{0.75}(TNR)\cdot H_2O$ complex. J Hazard Mater. 2005;A117:103–10.

42. Shamsipur M, Pourmortazavi SM, Hajimirsadeghi SS. Investigation on decomposition kinetics and thermal properties of copper fueled pyrotechnic compositions. Combust Sci Technol. 2011;183:575–87.

43. Ma H-X, Song J-R, Zhao F-Q, Hu RZ, Xiao H-M. Nonisothermal reaction kinetics and computational studies on the properties of 2,4,6,8-tetranitro-2,4,6,8-tetraazabicyclo [1, 3] onan-3,7-dione (TNPDU). J Chem Phys. 2007;A111:8642–9.

44. Tompa AS, Boswell RF. Thermal stability of a plastic bonded explosive. Thermochim Acta. 2000;357–358:169–75.

45. Criado JM, Perez-Maqueda LA, Sanchez-Jimenez PE. Dependence of the pre-exponential factor on temperature. J Therm Anal Calorim. 2005;82:671–5.

46. Fathollahi M, Behnejad H. A comparative study of thermal behaviors and kinetics analysis of the pyrotechnic compositions containing Mg and Al. J Therm Anal Calorim. 2015;120:1483–92.

47. ASTM E698. Test methods for Arrhenius kinetic constants for thermally unstable materials.

48. Starink MJ. The determination of activation energy from linear heating rate experiments: a comparison of the accuracy of isoconversion methods. Thermochim Acta. 2003;404:163–76.

49. Shamsipur M, Pourmortazavi SM, Hajimisadeghi SS, Atifeh SM. Effect of functional group on thermal stability of cellulose derivative energetic polymers. Fuel. 2012;95:394–9.

50. Ma H, Yan B, Li Z, Guan Y, Song J, Xu K, et al. Preparation, non-isothermal decomposition kinetics, heat capacity and adiabatic time-to-explosion of NTO. DNAZ. J Hazard Mater. 2009;169:1068–73.

51. Roduit B, Xia L, Folly P, Berger B, Mathieu J, Sarbach A, et al. The simulation of the thermal behavior of energetic materials based on DSC and HFC signals. J Therm Anal Calorim. 2008;93:143–52.

52. Abusaidi H, Ghaieni HR, Pourmortazavi SM, Motamed-Shariati SH. Effect of nitro content on thermal stability and decomposition kinetics of nitro-HTPB. J Therm Anal Calorim. 2016;124:935–41.

53. Pisharath S, Ang HG. Synthesis and thermal decomposition of GAP–Poly (BAMO) copolymer. Polym Degrad Stab. 2007;92(7):1365–77.

54. Rocco J, Lima J, Frutuoso A, Iha K, Ionashiro M, Matos J, et al. Thermal degradation of a composite solid propellant examined by DSC. J Therm Anal Calorim. 2004;75:551–7.

55. Wan-Fen Pu, Liu Peng-Gang, Li Yi-Bo, Jin Fa-Yang, Liu Zhe-Zhi. Thermal characteristics and combustion kinetics analysis of heavy crude oil catalyzed by metallic additives. Ind Eng Chem Res. 2015;54:11525–33.

56. Li Y, Chenxia K, Huang C, Cheng Y. Effect of MnC_2O_4 nanoparticles on the thermal decomposition of TEGDN/NC propellant. J Therm Anal Calorim. 2012;109:171–6.

57. Shamsipur M, Pourmortazavi SM, Fathollahi M. Kinetic parameters of binary iron/oxidant pyrolants. J Energy Mater. 2012;30:97–106.

58. Pourmortazavi SM, Rahimi-Nasrabadi M, Rai H, Jabbarzadeh Y, Javidan A. Effect of nanomaterials on thermal stability of 1,3,6,8-tetranitro carbazole. Cent Eur J Energy Mater. 2017;14:201–16.

59. Eslami A, Hosseini SG, Asadi V. The effect of microencapsulation with nitrocellulose on thermal properties of sodium azide particles. Prog Org Coat. 2009;65:269–74.

60. Olszak-Humienik M, Mozejko J. Thermodynamic functions of activated complexes created in thermal decomposition processes of sulphates. Thermochim Acta. 2000;344:73–9.

61. Pourmortazavi SM, Rahimi-Nasrabadi M, Kohsari I, Hajimirsadeghi SS. Non-isothermal kinetic studies on thermal decomposition of energetic materials. J Therm Anal Calorim. 2012;110:857–63.

62. Pickard JM. Critical ignition temperature. Thermochim Acta. 2002;392:37–40.

63. Tonglai Z, Rongzu H, Yi X, Fuping L. The estimation of critical temperatures of thermal explosion for energetic materials using non-isothermal DSC. Thermochim Acta. 1994;244:171–6.